AGU PUBLICATIONS

JGR

Journal of Geophysical Research: Oceans

RESEARCH ARTICLE

10.1002/2013JC009425

Key Points:
- Weaker Arctic sea ice causes increased annual mean ocean surface stress (+20%)
- Increasing open water area in summer yields momentum flux reduction (−7%)
- An optimal ice concentration of 80–90% amplifies momentum transfer threefold

Correspondence to:
T. Martin,
torge.martin@gmail.com

Citation:
Martin, T., M. Steele, and J. Zhang (2014), Seasonality and long-term trend of Arctic Ocean surface stress in a model, *J. Geophys. Res. Oceans*, *119*, 1723–1738, doi:10.1002/2013JC009425.

Received 11 SEP 2013
Accepted 17 FEB 2014
Accepted article online 21 FEB 2014
Published online 10 MAR 2014

Seasonality and long-term trend of Arctic Ocean surface stress in a model

Torge Martin[1], Michael Steele[1], and Jinlun Zhang[1]

[1]Polar Science Center, Applied Physics Laboratory, University of Washington, Seattle, Washington, USA

Abstract A numerical ocean sea-ice model is used to demonstrate that Arctic sea ice retreat affects momentum transfer into the ocean. A thinner and thus weaker ice cover is more easily forced by the wind, which increases the momentum flux. In contrast, increasing open water reduces momentum transfer because the ice surface provides greater drag than the open water surface. We introduce the concept of optimal ice concentration: momentum transfer increases with increasing ice concentration up to a point, beyond which frictional losses by floe interaction damp the transfer. For a common ice internal stress formulation, a concentration of 80–90% yields optimal amplification of momentum flux into the ocean. We study the seasonality and long-term evolution of Arctic Ocean surface stress over the years 1979–2012. Spring and fall feature optimal ice conditions for momentum transfer, but only in fall is the wind forcing at its maximum, yielding a peak basin-mean ocean surface stress of ~0.08 N/m^2. Since 1979, the basin-wide annual mean ocean surface stress has been increasing by 0.004 N/m^2/decade, and since 2000 by 0.006 N/m^2/decade. In contrast, summertime ocean surface stress has been decreasing at −0.002 N/m^2/decade. These trends are linked to the weakening of the ice cover in fall, winter and spring, and to an increase in open water fraction in summer, i.e., changes in momentum transfer rather than changes in wind forcing. In most areas, the number of days per year with optimal ice concentration is decreasing.

1. Introduction

The Arctic sea ice cover is currently undergoing dramatic changes. It is shrinking in thickness [e.g., *Kwok and Rothrock*, 2009] and extent [e.g., *Cavalieri and Parkinson*, 2012] and becoming more dynamic, with increased drift speeds and deformation rates [*Rampal et al*., 2009]. How does this affect the ocean underneath? Sea ice insulates the Arctic Ocean from direct interaction with the atmosphere and potentially damps internal waves [*Morison et al*., 1985; *Levine et al*., 1987; *Plueddemann et al*., 1998]. *Rainville and Woodgate* [2009] hypothesize that the Arctic Ocean will become more energetic if the current sea ice retreat continues, and that the enhanced mixing may affect water mass transformation and transport, which ultimately might impact subpolar regions. Further, mixing is essential to supply the euphotic zone with nutrients, which means that changes in the momentum influx into the Arctic Ocean would not only affect physical properties but also primary production. While sea ice retreat is found to be associated with ocean warming [*Steele et al*., 2008], increased levels of light [*Nicolaus et al*., 2012] and primary production [*Arrigo et al*., 2008], its effect on momentum transfer into the ocean has been poorly documented to date.

What governs the momentum flux into the Arctic Ocean? The surface wind is the ultimate driver of ocean surface currents, waves, and mixing [see *Rainville et al*., 2011, for a review] as well as sea ice motion [e.g., *Thorndike and Colony*, 1982]. However, sea ice can be an effective moderator of momentum transfer into the ocean because of its great rigidity. Great internal stress may decouple wind and sea ice motion [*Steele et al*., 1997]. Accordingly, observations show that the annual cycle of upper ocean motion resembles that of ice compactness [*Plueddemann et al*., 1998]. Further, the air drag over ice and open water vary for different reasons, e.g., ocean surface waves increase the drag as a function of wind speed [e.g., *Taylor and Yelland*, 2001], whereas surface roughness of sea ice is a function of its age and deformation state [*Guest and Davidson*, 1991]. The average air-ice drag may be two times greater than typical air-ocean drag, in particular at average wind speeds [*Large and Pond*, 1981; *Overland*, 1985; *Guest and Davidson*, 1991; *Fairall et al*., 2003]. Therefore, it is reasonable to split the air stress τ_{air} acting on the surface of an ice-ocean continuum into a contribution over open water (τ_{ao}) and over ice (τ_{ai}):

$$\vec{\tau}_{air} = (1 - A_i)\vec{\tau}_{ao} + A_i\vec{\tau}_{ai} \quad (1)$$

where A_i denotes the ice-covered area fraction also known as sea ice concentration.

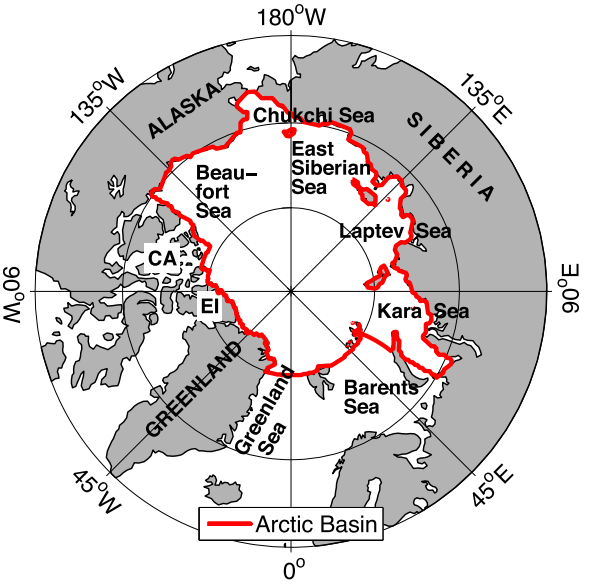

Figure 1. Map of the Arctic. The Arctic Basin is outlined by the bold red line. Labels name major marginal seas and land areas (capital letters); CA = Canadian Archipelago and EI = Ellesmere Island.

A near compact sea ice cover provides a resistive force against the motion forced by the wind. This internal stress may cause the ice floes to drift slower or to not move even in the presence of wind. The spatial gradient of the internal ice stress is called ice interaction force ($\boldsymbol{F}_i$).

Wind and sea ice drift exert a stress onto the ocean surface. While the air stress is commonly parameterized as a quadratic function of the wind velocity, the coupling of ice and ocean is more complicated. The ice-ocean stress can be approximated by a quadratic drag law as well [e.g., *Hibler*, 1979], but small-scale dynamics at the ice-ocean boundary are complex [*Morison and McPhee*, 2001; *McPhee*, 2002, 2012] and not resolved in common ocean sea-ice models. Most modelers thus rely on a constant ice-ocean drag coefficient for the quadratic drag parameterization that relates to the undisturbed (geostrophic) ocean current below the surface layer [*McPhee*, 1980]. However, this technique may require artificial damping in coupled ocean sea-ice models and strongly impacts the representation of inertial ice motion [*Hibler et al*., 2006]. *McPhee* [2012] argues that the ice-ocean drag relationship is not quadratic—proposing a Rossby similarity approach instead—with the drag dependent on ice type and speed as well as near-surface ocean stratification. Such feedbacks, however, are subject to future model improvement and validation, for which the observational effort also needs to be intensified, and beyond the scope of the present study. To avoid these complexities in this initial study, we follow *Hibler and Bryan* [1987] [as did e.g., *Kauker et al*., 2003; *Condron et al*., 2009; *Losch et al*., 2010] and compute the ocean surface stress τ_{ocn} as the vector sum of the air stress and the ice interaction force

$$\tau_{ocn} = \tau_{air} + \boldsymbol{F}_i \tag{2}$$

Here the ice interaction force is representative for a continuum of ice floes and open water and hence competes with the average air stress over this area and not only with the air-ice stress. The ice interaction force counteracts the air stress τ_{air}, i.e., its vector often points in the opposite direction [*Hibler and Bryan*, 1987; *Steele et al*., 1997], and has the potential to reduce the ocean surface stress. Hereafter, we refer to the magnitude of the stresses and forces if not stated otherwise.

Are there indications that the momentum influx to the ocean has recently changed? *Hakkinen et al*. [2008] and *Spreen et al*. [2011] reported on positive trends in surface wind stress and speed over the last 50 and 20 years, respectively. However, these increases were small, ~1–2% per decade, compared to the changes in sea ice characteristics. In the Arctic Basin (Figure 1), summer sea ice area decreased by 9% per decade from 1979 to 2010 [*Cavalieri and Parkinson*, 2012] and ice strength decreased by 37% between the periods 1979–2006 and 2007–2011 [*Zhang et al*., 2012].

In order to understand the consequences of a shrinking sea ice cover on the Arctic Ocean, it is important to deepen our knowledge of the momentum flux into the ocean and what governs its variability. Here we take a first step using an ocean sea-ice model simulation to investigate the impact of changing sea ice conditions on the transfer of momentum into the ocean. Using the modeled ocean surface stress as an indicator of momentum influx, we strive to answer the following questions: When and where is the ocean surface stress strongest in the Arctic over the course of a year? Did the surface stress magnitude as well as its spatial and seasonal characteristics change over the past three decades? What caused these changes?

This study is organized as follows: in section 2, we present relevant information on the ocean sea-ice model and model forcing. Section 3 contains results on the seasonality, long-term trend, and spatial distribution of basin-wide ocean surface stress as well as an analysis of causes for its change. These results are discussed in light of the special relationship of sea ice concentration and ocean surface stress in section 4, in which we also introduce the concept of an optimal ice concentration. We summarize our findings in section 5.

2. Model

This study is based on a simulation with the Pan-arctic Ice-Ocean Modeling and Assimilation System (PIOMAS) covering the period 1979–2012. The model grid covers the area north of 49°N and has an average horizontal resolution of 30 km in the Arctic Ocean, 30 vertical ocean levels—of which 10 are located in the top 60 m of the ocean—and 12 categories each for ice thickness, ice enthalpy, and snow depth [*Zhang and Rothrock*, 2003; *Zhang et al*., 2008]. The coupling of sea ice and ocean dynamics follows the approach of *Hibler and Bryan* [1987]. In this approach, the sea ice cover is embedded in the oceanic surface layer and the momentum balance of this layer comprises the surface stress as shown in equation (2). In order to compute the ice internal stress, the teardrop viscous-plastic rheology of *Zhang and Rothrock* [2005] is applied using an ice strength formulation as introduced by *Hibler* [1979]:

$$P = P^* h e^{-20(1-A_i)} \tag{3}$$

where P^* is a tunable sea ice strength parameter and h is the grid cell mean ice thickness.

The model is forced with atmospheric fields of the NCEP/NCAR reanalysis product [*Kalnay et al*., 1996], which includes 10 m wind velocity, 2 m air temperature, specific humidity, precipitation, evaporation, downwelling long-wave radiation, and cloud fraction. Air temperature and cloud fraction are used to calculate downwelling shortwave radiation following *Parkinson and Washington* [1979]. These fields feed into a one-dimensional atmospheric surface layer model that dynamically computes, among other quantities, the wind stress at the air-ocean and air-ice interfaces, the latter separately for each of the 12 ice categories, as described in *Briegleb et al*. [2004]. (For the ice-ocean exchange no comparable surface layer model is implemented and only fluxes integrated over all ice categories are communicated to the ocean component.) For wind speeds exceeding 3 m/s, the air-ice stress is greater than the air-ocean stress (Figure 2). At the basin-wide long-term mean wind speed of 4.5 m/s, for instance, the air-ice stress is twice as large as the air-ocean stress.

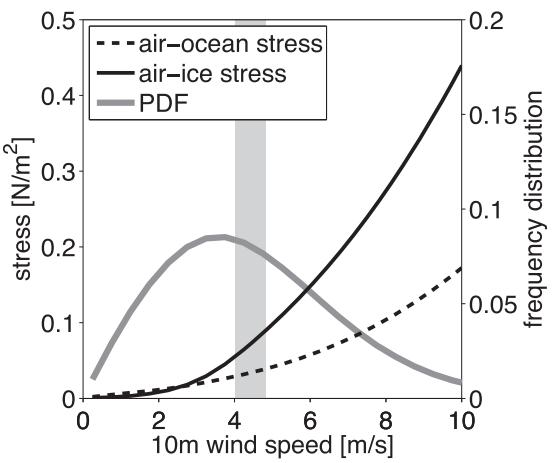

Figure 2. Magnitude of air-ocean stress τ_{ao} (dashed) and air-ice stress τ_{ai} (solid) as functions of wind speed at 10 m height. Daily data from the entire Arctic Basin (red outline in Figure 1) was binned with a bin width of 0.5 m/s. The black lines connect the respective bin averages considering year-round data from 1979 to 2012. The probability density function (PDF) of the daily wind speed is indicated by the bold gray line, which connects the individual frequency of occurrence of each wind speed bin. The gray shaded area indicates the range of monthly mean wind speed for the Arctic Basin, which is shifted to the right from the mode because the distribution is skewed toward higher wind speeds. Wind speed data are from NCEP reanalysis and are used to force the ocean sea-ice model.

Since we expect the areal retreat of the sea ice cover to be a major factor in momentum flux changes we used PIOMAS' assimilation capability [*Lindsay and Zhang*, 2006] to tie the sea ice edge—defined as the isoline of 15% ice concentration—in our simulation to observed sea ice concentrations provided by the National Snow and Ice Data Center (NSIDC) with daily resolution [*Nolin et al*., 1998]. PIOMAS results for sea ice drift and thickness were proven to agree well with observations [*Martin and Gerdes*, 2007; *Schweiger et al*., 2011]. For the model version used here *Zhang et al*. [2012]

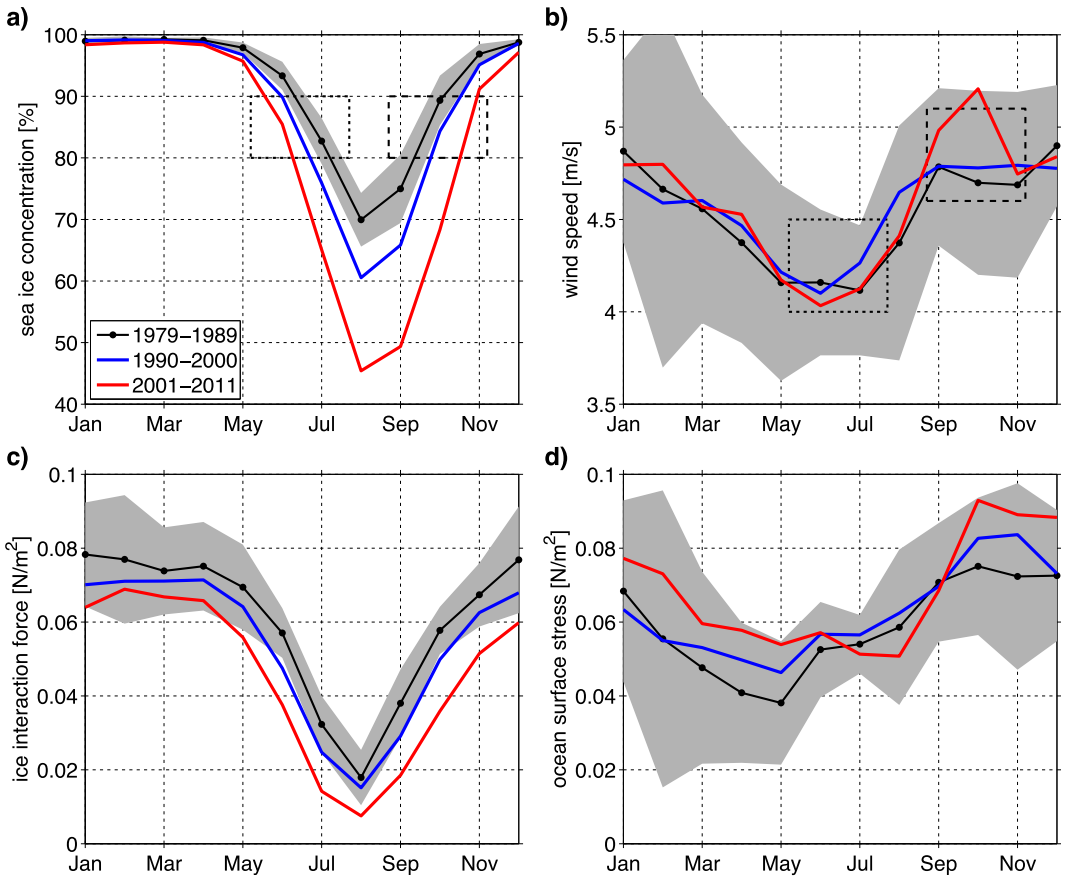

Figure 3. Annual cycles of monthly mean (a) sea ice concentration A_i, (b) surface wind speed at 10 m height from NCEP reanalysis, (c) ice interaction force magnitude F_i, and (d) ocean surface stress magnitude τ_{ocn} averaged over the Arctic Basin (see Figure 1). Black lines depict the annual cycle averaged over the period 1979–1989 with the gray shaded area indicating ±2 standard deviations. Blue and red lines depict the averages for the periods 1990–2000 and 2001–2011, respectively. Optimal ice concentrations (80–90%) enabling a maximization of the momentum flux into the ocean occur twice a year in spring (dotted box) and fall (dashed box).

give an ice thickness bias of 0.18 m with a correlation of 0.73 to observations from submarines, moorings, and airborne instruments for the period 1975–2008 and a bias of −0.1 cm/s for daily mean ice drift speed with a correlation of 0.80 to buoy drift estimates from 1979 to 2010. This model is very well validated for its momentum balance both in sea ice [*Kwok et al.*, 2008] and ocean [*Peralta-Ferriz et al.*, 2011].

3. Results

3.1. Seasonality

The ocean surface stress is a function of the surface wind, and hence can vary strongly from day to day. In order to reduce the noise and to focus on seasonality and long-term changes, we have computed seasonal averages defined as winter (January–March, JFM), spring (April–June, AMJ), summer (July–September, JAS), and fall (October–December, OND). These seasons follow the annual cycle of the Arctic sea ice cover in terms of its areal coverage represented by the sea ice concentration averaged over the Arctic Basin (Figure 3a). We define the Arctic Basin as the central Arctic Ocean plus the Beaufort, Chukchi, East Siberian, Laptev, and Kara seas, excluding the Barents Sea (Figure 1).

The annual cycle of ice concentration has a minimum of 70% in August for the early period 1979–1989 (Figure 3a). Refreezing begins in September and the ice concentration recovers during fall until reaching a maximum close to 100% in winter. The summer minimum decreased to 61% in the 1990s and further to 46% in the years 2001–2011. This means that during the most recent period, less than half of the Arctic Basin was ice covered at the height of summer. Further, the refreezing of the Arctic Basin takes longer and, for

instance, the October mean sea ice concentration of recent years barely reaches 70%, a value that used to mark the annual minimum during the early period.

Surface winds are weakest in spring and early summer and strongest in fall (Figure 3b). In contrast to the sea ice concentration, there is no significant change in the annual cycle of wind speed, i.e., the blue and red lines representing the 1990s and 2000s stay within the gray shaded area of ± 2 standard deviations of the 1980s, except for October in the 2000s. The latter can be explained by significantly ($\alpha < 0.01$) higher mean wind speeds in October 2005, 2007, and 2011. (This is in agreement with *Spreen et al*. [2011] and *Kwok et al*. [2013] who also find very weak wind speed trends over the period 1982–2009; they show offsetting trends for the three decades 1980s, 1990s, and 2000s.)

As shown by equation (2), the ice interaction force has the potential to damp the impact of the wind on the ocean. The annual cycle of the ice interaction force (Figure 3c) closely follows that of sea ice concentration (Figure 3a) because of the exponential increase of sea ice strength with ice concentration and only a linear dependence on ice thickness (equation (3)). In the first two decades, the ice interaction force is smallest in August at 0.02 N/m^2, increasing to 0.07–0.08 N/m^2 in winter. However, by the 2000s (red line), this force has declined between May and December by more than two standard deviations relative to 1980s values now having a summer minimum of only 0.008 N/m^2. The impact of this drastic change will be further discussed below.

The variability of ocean surface stress over time is a result of the combined variability of sea ice concentration, wind speed, and ice interaction force. The annual cycle of ocean stress (Figure 3d, black line) mostly resembles that of the wind speed. The ocean surface stress declines over winter, reaching a minimum of 0.037 N/m^2 in May. In summer, however, the ocean surface stress increases even though wind speeds stay low from May to July (Figure 3b). During this period, the steep seasonal decline of the ice interaction force (Figure 3c) enables a greater surface stress, despite weak winds, because now ice drift and wind are more closely coupled. The ocean surface stress reaches a maximum of 0.74 N/m^2 in October when wind speeds are 15–20% greater than in late spring and early summer.

In the 2000s, the annual cycle of the ocean stress changes. Now the minimum occurs later, in August, because the basin-wide mean ocean stress increases from the 1980s to the 2000s in all seasons except summer. In summer, in contrast to all other seasons, the ocean surface stress of the 2000s (Figure 3d, red line) falls below that of the 1980s (black line).

3.2. Long-Term Trend

Figure 4 shows time series of all terms of equations (1) and (2) covering the years 1979–2012. We show seasonal means of Arctic Basin-wide averages because of the pronounced seasonal variability of the ocean surface stress (Figure 3d). For the long-term trends of ice interaction force and ocean surface stress, the strong decline in ice thickness is of greater importance than variations in ice concentration, which is in contrast to the effects on the seasonal time scale discussed above. Nevertheless, the increasing fraction of open water within the Arctic Basin in summer plays an important role.

In winter, the sea ice concentration A_i is near 100% (Figure 4a, dashed black line), i.e., the entire Arctic Basin is ice covered. Consequently, the air-ocean stress weighted by the open water area $(1 - A_i)\tau_{ao}$ (dashed blue line) is negligibly small and the total air stress τ_{air} (solid blue line) is almost entirely determined by the ice area weighted air-ice stress $A_i\tau_{ai}$ (dashed green).

The magnitude of ocean surface stress (Figure 4, black line) is usually equal to or smaller than the total air stress (solid blue line), particularly in winter when the ice interaction force is strong. (Note that equation (2) is a vector equation and hence the air stress and ice interaction force magnitudes presented in Figure 4 do not necessarily add up to the ocean surface stress magnitude.) The total wintertime air stress does not feature a significant trend (Figure 4a, solid blue line), while the ice interaction force does (-0.0047 N/m^2/decade, red line). In particular, after 2000 the ice interaction force falls below one standard deviation of the years before 2000, and during five out of the last six winters it was about two standard deviations below the 1979–1999 mean. As a consequence of this reduced damping, the ocean surface stress increases by 0.0054 N/m^2/decade (solid black line), most strongly during the 2000s.

Trends in spring (Figure 4b) and fall (Figure 4d) basically resemble those of winter: the decline in ice interaction force (-0.0064 and -0.0090 N/m^2/decade) drives an increase in ocean surface stress (0.0051 and

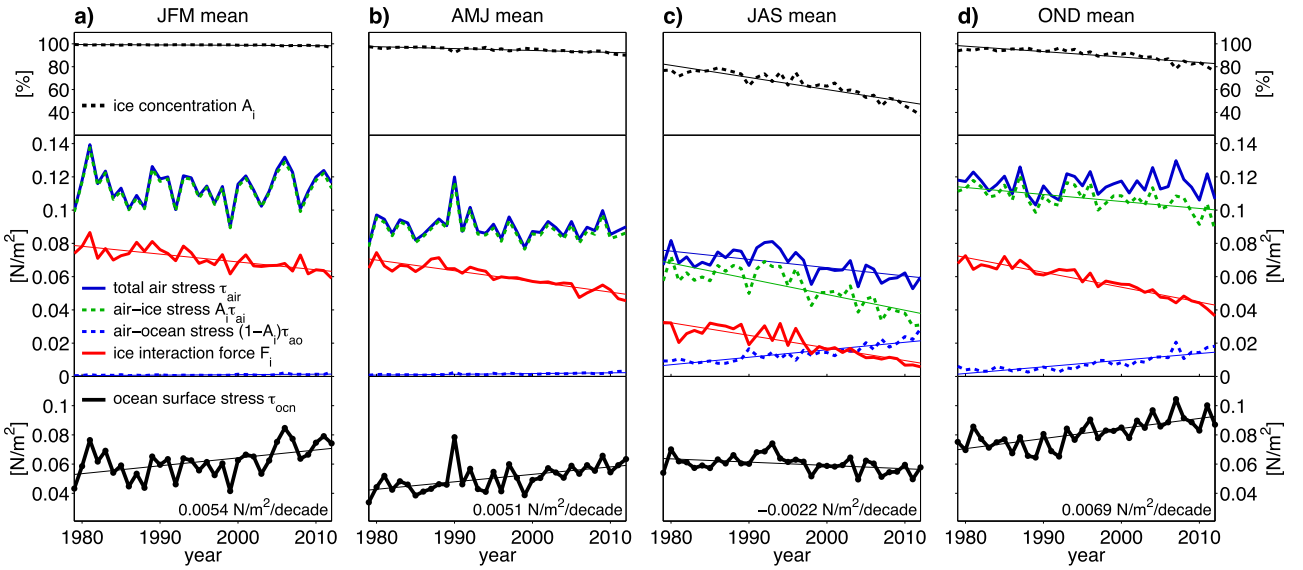

Figure 4. Arctic Basin averaged stress magnitudes (N/m^2) for seasonal means of (a) January–March, (b) April–June, (c) July–September, and (d) October–December for the period 1979–2012. (top row) The sea ice concentration A_i (dashed black line). (middle) Magnitudes of all components of equations (1) and (2): the weighted air-ice stress $A_i\tau_{ai}$ (dashed green), weighted air-ocean stress $(1 - A_i)\tau_{ao}$ (dashed blue), total air stress τ_{air} (solid blue), and the ice interaction force F_i (red). (bottom row) The magnitude of the resulting ocean surface stress τ_{ocn} is depicted in black. Thin straight lines indicate trends of the individual time series where the trend is significant at a level of 0.99, except for the ocean surface stress where the levels of significance are at 0.97 (JFM), 0.98 (AMJ), 0.94 (JAS), and 0.99 (OND). The legend in Figure 4a holds for all plots.

0.0069 N/m^2/decade). However, the total air stress is smaller in spring than in fall and winter, which matches the seasonal cycle of wind speeds presented in Figure 3b.

The positive shift in the ocean surface stress annual cycle in winter, spring, and fall from the 1980s to the 2000s (Figure 3d) is largely due to the decrease in ice interaction force (Figure 3c). The increase in the October maximum of the ocean surface stress of 0.018 N/m^2 from the 1980s to the 2000s (Figure 3d, black to red line) is a function of both, decreased ice interaction force (Figure 3c) and increased wind speeds in fall (Figure 3b). In particular, the strengthening of the wind forcing is exceptional in October of recent years as mentioned in section 3.1.

In summer, the situation is different: the ocean surface stress decreases by −0.0022 N/m^2/decade (Figure 4c, black line) though the ice interaction force declines (−0.0076 N/m^2/decade, red line) similar to all other seasons. Why is this? Unlike in any other season, the total air stress features a significant negative trend of −0.0050 N/m^2/decade in summer (solid blue line). As the climatology in Figure 3b shows this is not due to a change in wind speed. However, the sea ice area shrinks rapidly, exhibiting a trend of −10.6%/decade (Figure 4c, dashed black line). The change in ice area changes the partitioning between air-ice stress (dashed green line) and air-ocean stress (dashed blue line) from 6:1 in the 1980s to 1:1 in 2012. The ice area decline has such a great effect because the basin-wide mean air-ocean stress (τ_{ao}) amounts to less than half the air-ice stress (τ_{ai}) with 0.035 N/m^2 compared to 0.085 N/m^2 (cf. Figure 2). The decline in ice interaction force has less impact, since this force is generally small in summer amounting to a third of its winter value in the 1980s and only a sixth in most recent years. As a result, the ocean surface stress decreases in summer.

A notable consequence is that the summer ocean surface stress, which was larger than in spring in the 1980s and 1990s, now is less than in spring (cf. Figures 4b and 4c, solid black lines). Moreover, the summer ocean surface stress is very close to the total air stress in recent years with a difference of less than 0.005 N/m^2 in any of the last 10 years and only 0.002 N/m^2 in 2012.

We speculate that the decline in summer mean ocean surface stress may extend into spring and fall over the coming years. Focusing on fall (Figure 4d), we find that the contribution of the air-ice stress (dashed green line) to the total air stress (solid blue line) decreased, while that of air-ocean stress (dashed blue line) increased over the last 15 years. Just like in summer, the weaker air-ocean stress gains weight in the sum

forming the total air stress because the sea ice concentration decreases at −4.8%/decade in fall. Further, the ice interaction force in fall continuously declines and drops below 0.04 N/m^2 for the first time in 2012 approaching values that are typical for summer. A similar tendency becomes visible in spring during the last ∼5 years of our model run though the signal is still weak. However, increased wind speeds during fall of recent years (Figure 3b, red line) can mask or delay the decline and possible reversal of the ocean surface stress trend.

3.3. Spatial Patterns

Surface winds and sea ice characteristics have great spatial heterogeneity, and so has the ocean surface stress. In Figure 5, we present maps of seasonally averaged ocean surface stress magnitude averaged over the period 1979–1989 (left column) and departures from this mean in the 1990s and 2000s (middle and right columns). Despite the seasonally changing magnitude, the spatial pattern of ocean stress is similar in all seasons: minima are located north of Greenland and the Canadian Archipelago and on the Siberian shelves, most prominently in the East Siberian Sea (see labels on map in Figure 1). We find maxima in the Greenland and Barents seas as well as in the Chukchi Sea. Within the Arctic Basin, there is a belt of enhanced ocean stress stretching from the Beaufort/Chukchi Sea along and north of the shelf seas into the Transpolar Drift Stream. The latter forms together with the Beaufort Gyre, the dominant pattern of sea ice drift [e.g., *Martin and Gerdes*, 2007]. However, unlike with the Transpolar Drift Stream there is no particular pattern of ocean surface stress that could be associated with the Beaufort Gyre.

The minimum just north of Greenland and Ellesmere Island, a region tending toward high sea level pressure, is related to high ice strength and low wind speeds averaging at less than 4 m/s in all seasons (Figure 6). Seasonally averaged wind speeds are also not particularly strong (<4.5 m/s) in most parts of the central Arctic Ocean. In addition, the ice cover is thick and compact in the 1980s, even in summer (Figure 7). Although winds are stronger along the Siberian coast, the model simulation features particularly thick ice in the East Siberian Sea in the 1980s, which causes higher than average ice interaction forces and thus does not pass the wind stress on to the ocean. Wind speeds in the Laptev and Kara seas are higher, reaching seasonal mean speeds of 5–6.5 m/s (Figure 6). The Greenland and Barents seas as well as the Chukchi Sea feature even stronger winds of more than 8 m/s.

From Figure 3, we concluded that basin-wide mean ocean stress increases from spring to summer despite weak winds because the ice interaction force weakens considerably. Comparing the spatial distributions of ocean surface stress in spring and summer (Figure 5, left column) we find greatest stress increases in the marginal ice zone area ($15\% \leq A_i \leq 85\%$; Figure 7a, left), which expands during summer. Ocean surface stresses are greatest in the marginal ice zone because sea ice in free drift has the potential to transfer the most momentum (see section 4). The resulting band of high stress in this area is a product of averaging over several years and is not as prominent in any given year.

The middle and right columns of Figure 5 show the seasonally averaged differences in ocean surface stress in the 1990s and 2000s from the 1980s mean ocean stress displayed in the left column. The dominating pattern is a general increase in ocean surface stress in most parts of the Arctic. In agreement with the opposing negative summer long-term trend presented in Figure 4, the summer pattern is different from the other seasons. Despite the increase in ocean surface stress (red colors) in the central Arctic, where there is perennial sea ice even in the 2000s, there is a decrease in ocean surface stress (blue colors) over a wide area stretching from the Beaufort Sea along the Siberian shelf to the Barents Sea. Since there is no general decrease in wind speed in this area (Figure 6b), we conclude that this ocean surface stress reduction is caused by the increasing amount of open water (Figure 7a) and increasing length of the ice-free season in this area. As pointed out above, there is generally less momentum transferred into the ocean through the open water surface than through the rougher sea ice.

In contrast, the decrease in ocean surface stress in the Laptev Sea in winter is related to a negative trend in the wind forcing (Figure 6a), which is inherent to several reanalysis data sets but particularly strong in the one used here [*Spreen et al.*, 2011]. Similarly, the strong increase in ocean surface stress over the Arctic Basin in fall is partly due to higher wind speeds, in particular in the 2000s as mentioned above.

Another interesting case is the East Siberian Sea. While our simulation features sea ice as thick as 5 m and 2.5 m in winter and summer, respectively, in this region in the 1980s, the thickness decreases to less than

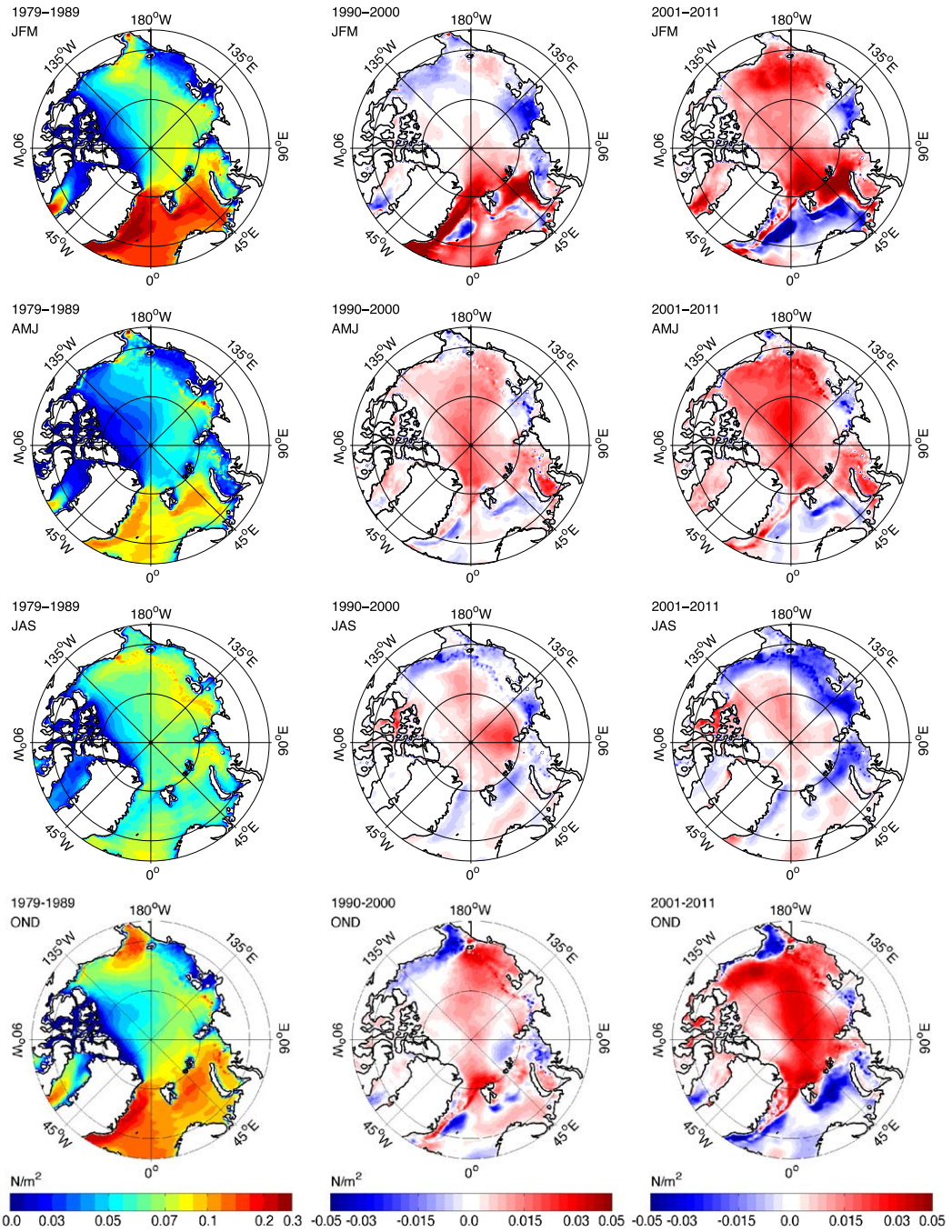

Figure 5. (left) Maps of seasonally averaged ocean surface stress magnitude for the period 1979–1989 and maps of the difference in ocean surface stress magnitude to this first period for (middle) 1990–2000 and (right) 2001–2011. The four seasons are: January–March (JFM, top row), April–June (AMJ, second row), July–September (JAS, third row), and October–December (OND, bottom row). The color bars at the bottom hold for all plots in the respective column.

2.5 m and 1 m during the 1990s (Figure 7b). It is the region with the by far steepest decline in ice thickness. This trend continues into the 2000s when finally this region becomes mostly ice free in summer. This change in ice thickness causes a decline in ice interaction force that is unique for the Arctic Basin in its steepness and persistence. As a consequence, the ocean surface stress declines in summer in the 2000s but increases in all other seasons in this region, which is consistent with the mechanisms outlined above. There is no equivalent trend in wind speed that would explain this evolution in ocean surface stress. However, our

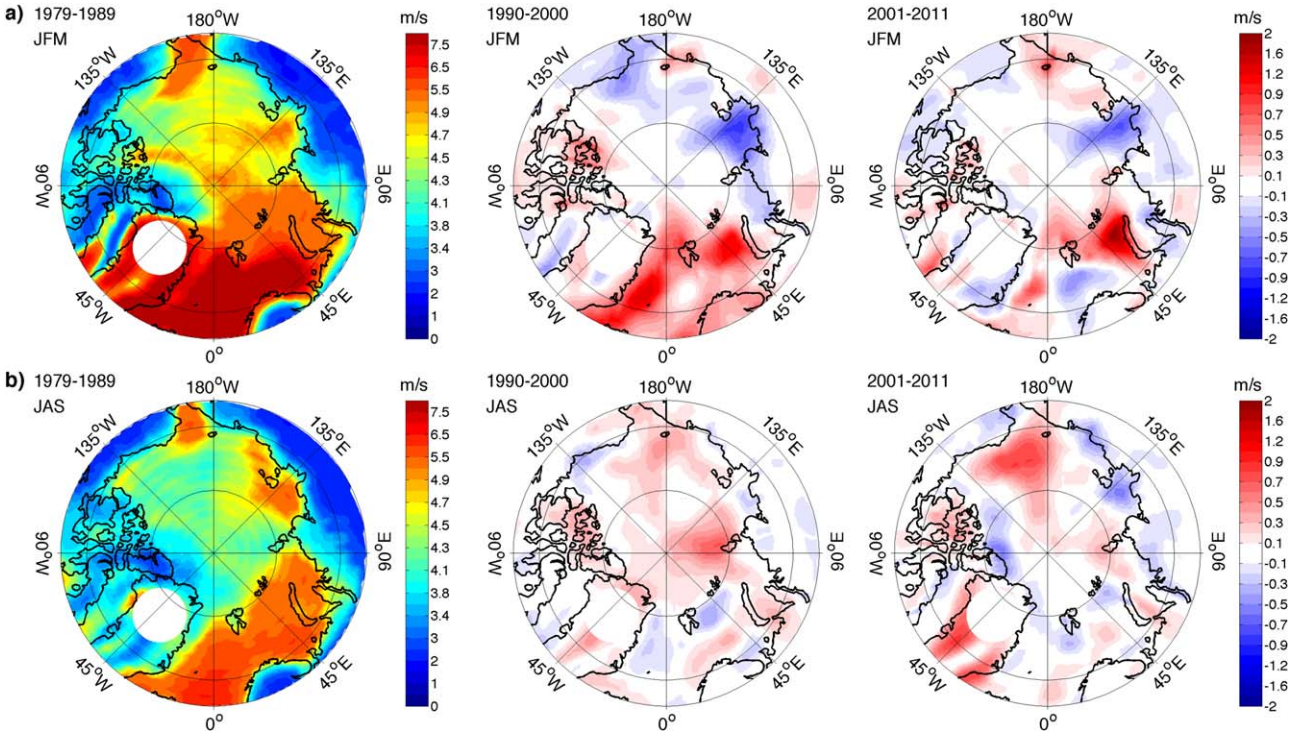

Figure 6. Maps of seasonally averaged wind speed for (a) winter and (b) summer for the period (left) 1979–1989 and deviations from these for the periods (middle) 1990–2000 and (right) 2001–2011. 10 m wind velocities from the NCEP/NCAR reanalysis were regridded onto the PIOMAS grid.

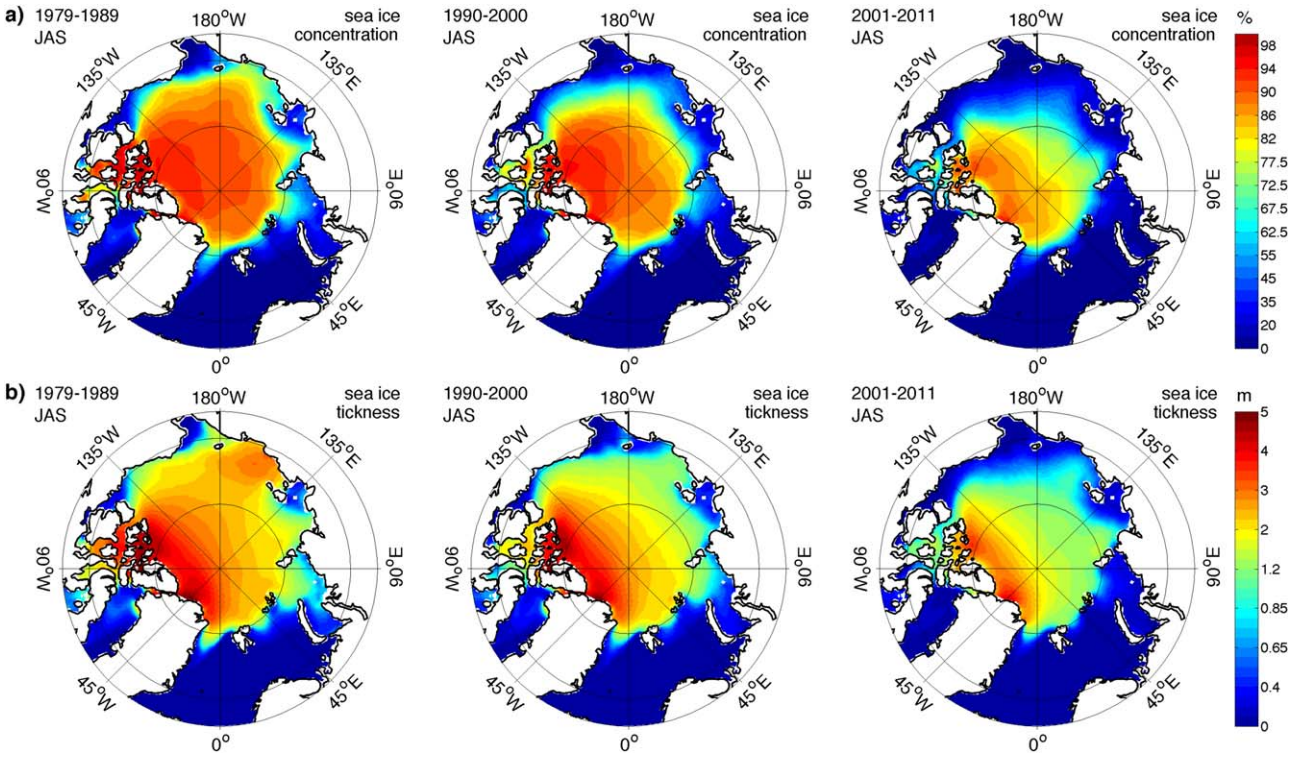

Figure 7. Maps of summer mean (July–September) (a) sea ice concentration and (b) thickness for three consecutive periods 1979–1989, 1990–2000, and 2001–2011.

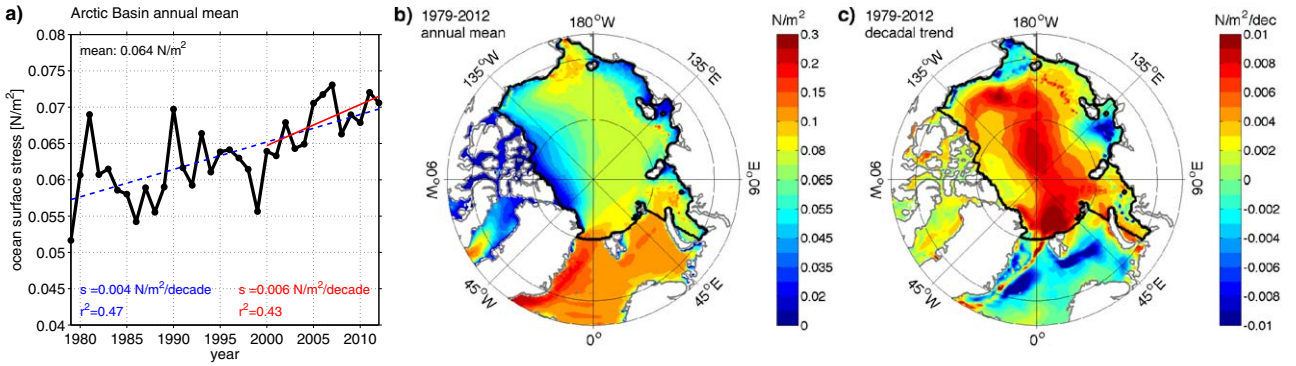

Figure 8. (a) Time series of annual mean ocean surface stress (N/m^2) averaged over the Arctic Basin (see bold black outline in maps on right); the dashed blue line depicts the linear trend for the period 1979–2012 and the red line the trend for 2000–2012, which both are significant at a level of 0.99; trend slopes *s* and explained variance r^2 are both printed in the plot for each trend in the respective color. (b) Map of annual mean ocean surface stress (N/m^2). (c) Map of local long-term (1979–2012) trends based on annual mean ocean surface stress (N/m^2/decade).

simulation results may be biased by the fact that we do not explicitly model land-fast ice [*Johnson et al.*, 2012]. In general, land-fast ice would hamper momentum transfer in the coastal regions of the shelf seas.

3.4. Annual Mean Distribution and Trends

To summarize the findings presented in this section, we show in Figure 8 the time series of the annual mean ocean surface stress for the Arctic Basin and maps of the long-term (1979–2012) annual mean ocean surface stress as well as local trends derived from time series of annual means. The basin-wide long-term mean ocean surface stress amounts to 0.064 N/m^2; its temporal evolution over the time period 1979–2012 features a significant positive trend of 0.004 N/m^2/decade over the Arctic Basin (Figure 8a). This means that on average the momentum influx into the Arctic Ocean increased by more than 20% over the last three decades. The trend has even steepened to 0.006 N/m^2/decade over the last 12 years (red line in Figure 8a). However, the time series also shows strong interannual variations, and the linear trend thus only explains 47% of the overall variability.

Spatially, the annual mean ocean surface stress varies between 0.04 N/m^2 and 0.08 N/m^2 in most parts of the Arctic Basin with maxima of up to 0.15 N/m^2 in the Chukchi, Laptev and Kara seas (Figure 8b). Greater ocean surface stresses are found in the Barents and Greenland seas where the annual mean can be as high as 0.25 N/m^2. The ocean surface stress is smallest along the coasts, most prominently north of Greenland as well as the Canadian Archipelago and on the Siberian shelf, in particular in the East Siberian Sea, for reasons discussed above. This distribution shapes a gradient of decreasing ocean surface stress toward Greenland and the Canadian Archipelago for the interior Arctic Ocean.

The long-term trend in annual mean ocean surface stress varies spatially as well, not only in steepness (0.001–0.01 N/m^2/decade) but also in sign. Although the trend is largely positive over the Arctic Basin, there are a few regions, such as the Laptev and Chukchi seas, where ocean surface stress is decreasing. The spatial pattern of the annual mean trends particularly resembles the spatial distribution of the stress differences in fall between the 1980s and 2000s (Figure 5, bottom right). This highlights the increasing weakness and inability of the diminished sea ice cover (Figure 7) to shield the ocean from high wind speeds in fall (Figure 3b). Anomalous negative trends in the Laptev and Chukchi seas can be explained by reductions in wind forcing (Figure 6) and ice season length, respectively.

4. Optimal Ice Concentration

Figure 2 indicates that sea ice has the potential to transfer more momentum into the ocean than is transferred when the wind acts directly on the water surface. Can we find this effect of momentum flux amplification by sea ice in our simulation? And to what extent does the ice interaction force damp this amplification?

In Figure 9a, we show the modeled mean ocean surface stress as a function of sea ice concentration (black line). For ice-free conditions, the model simulates an ocean surface stress of ~0.04 N/m^2, which compares

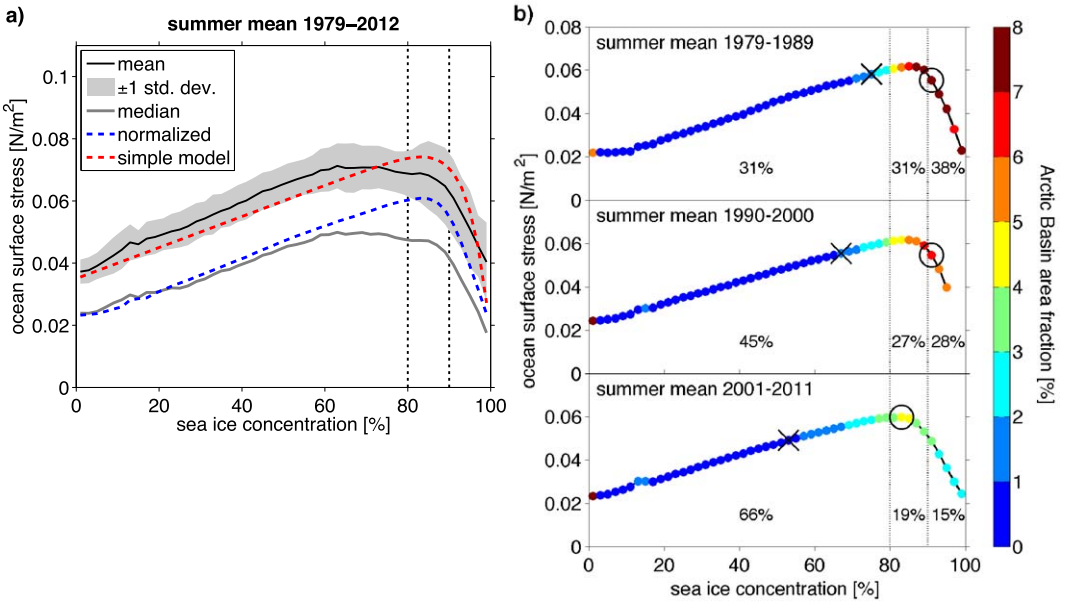

Figure 9. (a) Ocean surface stress as a function of sea ice concentration. Sea ice concentration over the entire Arctic Basin (see Figure 1) from daily model output was binned using a bin width of 2%. For each bin, the mean and median ocean stresses were calculated—weighted by grid cell area—for the summer months July–September for each year of the period 1979–2012. The solid black line depicts the bin-mean ocean stress considering summer means from all 34 years. Gray shading marks the ±1 standard deviation from individual year summer means. The lower dark gray line depicts the median ocean stress averaged over all 34 years. The dashed blue line depicts the median ocean surface stress normalized by the square of the daily wind speed. The simple model of equation (4) is depicted as a dashed red curve. (b) Arctic Basin summer median ocean surface stress adjusted for wind speed (cf. dashed blue line in Figure 9a) for three consecutive 11 year periods. Colored dots indicate the frequency of occurrence for each bin in terms of the total area fraction (%) of the Arctic Basin covered by all grid cells sorted into the respective bin. Note the first bin on the left includes open water. The mean and mode of the ice concentration distribution are marked by a cross "x" and a circle "o," respectively, in each plot. Percentages printed in each plot note the area fraction of the Arctic Basin covered by ice concentrations of 0–80%, 80–90%, and 90–100% (sections separated by vertical dashed lines).

well with global estimates outside of the Westerlies [e.g., *Gille*, 2005]. The stress clearly increases with increasing ice concentration but only to an ice concentration of about 60% where it levels off at ~0.07 N/m^2. The stress declines steeply for ice concentrations greater than 85%. We binned daily model output from July to September with respect to sea ice concentration (bin width 2%) and calculated the mean and the median ocean surface stresses for each bin. The black line connects the bin means averaged over all 34 years of our simulation; the interannual variability of the bin mean is small as indicated by the standard deviation (gray shaded area). The variability of the daily data in each bin is greater as the difference between mean and median (gray line) shows. In the following, we focus on the median because it is less affected by extreme values within each bin.

Wind speeds, however, are not uniformly distributed across ice concentrations and the black and gray curves include variability of the wind forcing. We, therefore, present another estimate of the relationship adjusted for wind speed depicted by the dashed blue curve in Figure 9a: we divide the ocean surface stress by the square of the wind speed on a daily basis and multiply the resulting bin median stress by the square of the basin-wide long-term mean wind speed, which is (4.5 m/s)^2, to obtain the same units. The normalized median ocean surface stress now shows a prominent peak at 85% ice concentration (dashed blue curve).

What shapes the ice-concentration ocean-stress relationship? Two fundamental model assumptions lead the way: First, the surface roughness of sea ice is generally greater than that of open water (Figure 2) and hence the ocean receives more momentum the more ice is present. Second, this only holds true for ice floes in free drift, i.e., the ice interaction force being negligibly small ($|\boldsymbol{F}_i| \sim 0$). Following the approach of *Hibler* [1979], the ice interaction force is virtually zero below an ice concentration of ~80% and increases exponentially with ice concentration (equation (3)).

To visualize the effect of these two model assumptions we take a third approach on the relationship: We insert equation (1) into equation (2) and apply average summer values for the air-ice and air-ocean stresses of 0.085 N/m^2 and 0.035 N/m^2, respectively, and a summer maximum value of 0.07 N/m^2 for the ice

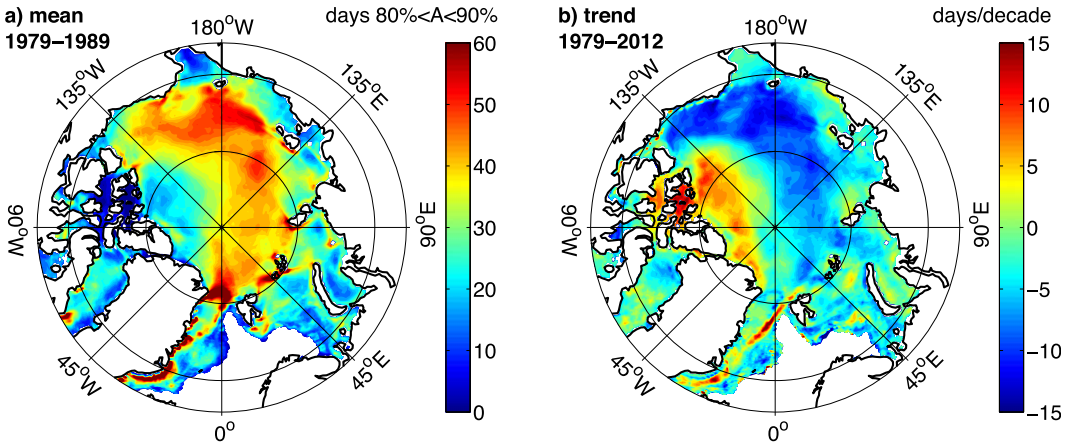

Figure 10. (a) Number of days per year with ice concentrations between 80 and 90% (see segment framed by dashed black lines in Figure 9a). An average over the period 1979–1989 is shown. (b) Linear trend in number of days with ice concentrations between 80 and 90% for the period 1979–2012.

interaction force. The latter we scale exponentially with ice concentration A_i similar to equation (3). This yields the following simple model equation in which the ocean surface stress τ_{ocn} is only a function of the ice concentration A_i

$$\tau_{ocn}(A_i) = 0.05\,\mathrm{N/m^2}\,A_i + 0.035\,\mathrm{N/m^2} - 0.07\,\mathrm{N/m^2}\,e^{-20(1-A_i)} \tag{4}$$

Here we assume that the ice interaction force counteracts the wind stress, i.e., we subtract its magnitude. We quickly see the two major effects of sea ice concentration: ocean surface stress increases linearly with increasing sea ice concentration because ice is rougher than water; however, once the floes freeze together to form a rigid sea ice cover, the momentum transfer is damped by the increasing ice interaction force—the ice motion decouples from the wind for great ice concentrations and the ocean receives less momentum (dashed red line in Figure 9a). The ocean receives some momentum even at very high ice concentrations (>98%) because the pack ice may move uniformly as a compact floe aggregate, whose horizontal dimensions exceed the grid scale, and hence transfers some momentum even if the local ice interaction force is greater than the local wind stress. Note, the slope of the linear increase of ocean surface stress for ice concentrations smaller then 80% and the location of a peak between 80 and 90% of the normalized ocean surface stress (blue curve) from PIOMAS output agree very well with this simple model (red curve).

Figure 10a shows a map of the number of days per year with ice concentrations between 80 and 90% averaged over the period 1979–1989. These optimal ice concentrations are associated with maximum momentum flux (vertical dashed black lines in Figure 9a). The region of greatest ocean surface stress (Figure 5, left column) generally coincides with the area of most days with optimal ice concentration. In the 1980s, there is a strong gradient in the number of days with such optimal ice conditions across the Arctic Basin from Greenland toward Siberia. This gradient roughly follows the distribution of ice thickness (Figure 7b). However, reasons for reduced ocean surface stress differ: the Siberian shelf seas feature more open water and fewer days within the optimal ice concentration range and thus fall into a regime being located left of the vertical dashed lines in Figure 9a, whereas in the area north of Greenland the ice is too thick and compact and thus rarely in free drift, which characterizes the regimes to the right of the vertical dashed lines in Figure 9a.

Relative to an ice-free ocean, the presence of sea ice amplifies the amount of wind stress that is transmitted to the ocean. We may define three stages of amplification that depend on the ice concentration: weak amplification ($A_i < 80\%$), optimal amplification ($80\% \leq A_i \leq 90\%$), and damped amplification ($A_i > 90\%$). In many places, Arctic sea ice cycles through these three stages with the annual cycle of sea ice concentration (cf. Figure 3a, dotted and dashed boxes mark periods of optimal amplification). Figure 9b displays the effect of the long-term downward trend in sea ice concentration on the ocean surface stress in the Arctic Basin in terms of optimal ice concentration. The three lines resemble the blue dashed line in Figure 9a, the median

summer ocean surface stress adjusted for wind speed as a function of sea ice concentration, but separate for the three periods 1979–1989, 1990–2000, and 2001–2011. The color-filled circles depict the frequency of occurrence for each ice concentration bin based on daily data over the entire Arctic Basin. Since the grid cell area of the model varies, the frequency of occurrence is expressed as the area fraction of the Arctic Basin that is covered by the respective ice concentration; the fractional areas (color-filled circles) add up to 100% in each of the three plots.

The long-term decrease in high sea ice concentrations in summer is evident in both, the shift of the overall mean (marked by a black cross in each plot of Figure 9b) toward lower concentrations and the shift in color for ice concentrations exceeding 85% from dark red to orange to green from the 1980 to the 1990s to the 2000s. While the mode of the ice concentration distribution (black circle) did not change between the 1980s and 1990s, it is located within the range of optimal ice concentration in the 2000s. However, the total area that is covered by optimal ice concentrations has actually decreased from 31% in the 1980 to 19% in the 2000s, which matches the negative trend of the basin mean depicted in Figure 4c. In addition, Figure 9b illustrates that in the 1980s momentum transfer was less than optimal because it was damped by the ice interaction force (38% of the Arctic Basin had ice concentrations exceeding 90% even in summer), whereas the momentum influx in recent summers has decreased strongly because of the increased open water fraction (66% of the Arctic Basin has less than 80% ice coverage). In other words, while most of the Arctic Ocean was in the damped amplifier regime even in summer in the early decades, it is dominated by the weak amplifier regime in recent summers. Figure 9b also demonstrates that the great regional differences in ocean surface stress in summer (Figure 5, third row) are not only caused by wind speed variations (cf. Figure 6b) but strongly depend on the compactness of the ice cover (cf. Figure 7a). With model predictions indicating a continuation of the decline in sea ice area, the ocean surface stress may also continue to decrease in summer. There will be local differences and also exceptional years since ice concentration and wind speed vary on a synoptic scale with the atmospheric circulation, but the mean trend will likely be negative.

Analogously, the spatial distribution of the number of days with optimal ice concentration changed over the past two decades. Vast areas of the Arctic Basin that had favorable conditions in the 1980s (cf. Figure 10a) feature a negative trend, losing up to 15 days with optimal ice concentration per decade (Figure 10b). In contrast, the area north of Greenland and the Canadian Archipelago, which used to be characterized by thick, compact multiyear ice, now tends toward more days with a looser ice pack yielding a greater momentum flux.

We note that our findings are tied to the particular model we use. However, the model physics of importance to our study are those used in many state-of-the-art climate models, while this particular model's ability to reproduce a variety of observations has been shown by many previous studies [e.g., *Martin and Gerdes*, 2007; *Peralta-Ferriz et al*., 2011; *Schweiger et al*., 2011]. Some models use an alternate form of ice-ocean momentum coupling, replacing the right-hand side of equation (2) with ice concentration-weighted air-ocean and ice-ocean stresses, the latter being a function of quadratic terms that depend explicitly on ice and ocean velocities [e.g., *Hibler*, 1979]. We here simply note that *Losch et al*. [2010] recently found a difference in mean sea ice drift speed between the two parameterizations of about 10%.

Our model (like all models) neglects some physical effects which might impact our results. For example, the underside roughness of multiyear ice is estimated to be an order of magnitude greater than that of first-year ice [*McPhee*, 2012], which has become the dominant ice type in the Arctic [*Rigor and Wallace*, 2004; *Kwok and Untersteiner*, 2011]. Further, extensive sea ice melt and the accumulation of melt water under the ice has a "lubricating" effect, because it creates a highly stratified ocean surface layer; this accelerates ice motion and reduces momentum transfer into the ocean [*McPhee*, 2002, 2012, 2013]. The net effect of these changes might be a further reduction in ocean surface stress not accounted for in our study.

Further, the surface roughness of sea ice at the air-ice interface varies with the age and deformation state of the ice as well [*Guest and Davidson*, 1991]. Our simulation does not account for this variability; rather, it assigns a single surface roughness for all ice, which is a combination of both skin and form drag. Measurements in the marginal ice zone have revealed that the total air drag is greatest at 50–60% ice concentration [*Birnbaum and Lüpkes*, 2002; *Andreas et al*., 2010; *Lüpkes et al*., 2012]. Thus, accounting for the dependency of the form drag on the ice concentration (effect of floe edges) and deformation state (ridges) would likely shift or broaden the range of optimal ice concentration toward lower values.

It is beyond the scope of this study to assess the impact of all these processes, in particular since measurements and fitted parameterizations of air-ice drag show considerable scatter [*Lüpkes et al*., 2012] and ice-ocean drag measurements are sparse [e.g., *McPhee*, 2002]. Nevertheless, work on atmosphere-ice-ocean coupling based on in situ measurements and simple models has greatly advanced in recent years and deserves to receive even greater attention by the large-scale modeling community in the future. We suspect that, in spite of our model's shortcomings, the concept of an optimal ice concentration somewhere between 0 and 100% for which momentum transfer into the ocean is maximal, is robust.

5. Conclusions

The Arctic sea ice cover has been shrinking for several decades. As a result, large areas of the Arctic Ocean have become ice-free in summer, affecting the momentum flux into the Arctic Ocean. The ultimate source of momentum to the ocean is the wind, whose variability dominates both annual cycle and interannual variability of the ocean surface stress. However, our study shows that the momentum transfer into the ocean is strongly controlled by the sea ice conditions on seasonal as well as decadal time scales. For instance, the decreasing compactness and weakening of the ice cover in spring enables an early recovery of the momentum influx during summer before wind speeds pick up in fall.

The average ocean surface stress has changed significantly during the past decades by 0.004 N/m^2/decade on annual average or 20% over the period 1979–2012. The exact trend as well as the ocean surface stress magnitude are, however, probably dependent on the particular model we use. The increase in surface stress is not obvious from the wind forcing thus indicating a change in momentum transfer rather than available momentum. However, the long-term trend of the momentum flux into the ocean is not positive in all seasons. It is governed by two contradicting effects, which both have their origin in Arctic sea ice loss: The thinning trend of the sea ice makes it weaker and less resistive against the wind forcing, which enables an increase in momentum transfer of 25% in fall, winter, and spring between the 1980s and 2000s. In contrast, once the ocean becomes predominantly ice-free, the average surface air stress decreases because the stress on open water amounts to less than half the stress on sea ice and thus open water transfers less momentum into the ocean. Hence, the decreasing sea ice extent in summer causes a decrease in ocean surface stress of 7% between the 1980s and 2000s. In summary, sea ice concentration dominates the annual cycle of the ocean surface stress and ice thickness its long-term evolution. In total, more momentum was transferred into the ocean during the last decade though the trend is negative in summer. This negative trend will eventually spread into early fall and late spring during the next decades.

Our conclusions refer to basin-wide, seasonal mean surface stresses and hence do not necessarily contradict the finding of *Rainville and Woodgate* [2009] that individual strong wind events can intensify mixing locally in ice-free areas. However, these sporadic events will likely not revert the overall trend of a decreasing ocean surface stress in summer caused by the lack of sea ice. For instance, the great cyclone of summer 2012 [*Simmonds and Rudeva*, 2012] did not leave a significant imprint on the basin-wide seasonal mean ocean surface stress (see Figure 4c). Nevertheless, the increasing strength of Arctic summer cyclones [*Simmonds and Keay*, 2009] may reduce the magnitude of the negative summer trend at some point by increasing the wind forcing.

Our analysis indicates that sea ice in free-drift amplifies the momentum transfer from the atmosphere into the ocean, which contradicts the general perception that sea ice damps the atmosphere-ocean exchange. Our simulation yields a long-term (1979–2012) basin-wide mean ocean surface stress of 0.064 N/m^2. On annual average, most momentum is transferred at an ice concentration of 85%, this is 0.076 N/m^2 considering a mean wind speed of 4.5 m/s, which again depends on the model used here. On the seasonal scale, sea ice conditions are optimal for maximal momentum flux into the ocean twice a year, in spring and fall. However, wind speeds are much higher in fall, yielding basin-mean ocean surface stresses of up to 0.1 N/m^2. This maximum was reached in fall 2007 and 2011. Due to the retreat of the sea ice cover during the past two decades, the region that experiences these favorable sea ice conditions for more than 30 days per year shifts from near the continental shelves into the interior Arctic Ocean and further toward Greenland and the Canadian coastline.

A region of great changes and thus particular interest for future study is the Befaufort Sea, where a decrease in ice interaction force facilitates accelerated ice motion [*Spreen et al*., 2011], increased momentum transfer

into the ocean (this study), and stronger downwelling within the Beaufort Gyre and upwelling along the coast [*Yang*, 2009]. Further, the increased accumulation of freshwater within the gyre has led to enhanced geostrophic currents along its periphery [*McPhee*, 2013]. The latter may significantly affect the ice and surface ocean momentum balance, in particular in the absence of strong winds, and thus also impact momentum transfer, downwelling, and freshwater accumulation.

The increasing occurrence of ice-free conditions in summer and fall may make observations of upper ocean properties easier. However, intensified measurements in the extended marginal ice zone ($15\% \leq A_i \leq 85\%$) and thin ice will be necessary to understand changes in momentum transfer related to changing ice and ocean characteristics and to prove or disprove conclusions drawn from complex though still limited numerical models.

Acknowledgments
This study was funded by the National Science Foundation (NSF ARC-1203240 and ARC-0901987). We thank Jiayan Yang and an anonymous reviewer for their helpful comments, which lead to an improved discussion of our results in light of present theory and observations.

References

Andreas, E. L., T. W. Horst, A. A. Grachev, P. O. G. Persson, C. W. Fairall, P. S. Guest, and R. E. Jordan (2010), Parametrizing turbulent exchange over summer sea ice and the marginal ice zone, *Q. J. R. Meteorol. Soc.*, *136*(649), 927–943, doi:10.1002/qj.618.

Arrigo, K. R., G. van Dijken, and S. Pabi (2008), Impact of a shrinking Arctic ice cover on marine primary production, *Geophys. Res. Lett.*, *35*, L19603, doi:10.1029/2008GL035028.

Birnbaum, G., and C. Lüpkes (2002), A new parameterization of surface drag in the marginal sea ice zone, *Tellus, Ser. A*, *54*, 107–123.

Briegleb, B. P., C. M. Bitz, E. C. Hunke, W. H. Lipscomb, M. M. Holland, J. L. Schramm, and R. E. Moritz (2004), Scientific description of the sea ice component in the community climate model, version 3, *Tech. Note NCAR/TN-463+STR*, 78 pp., Natl. Cent. for Atmos. Res., Boulder, Colo.

Cavalieri, D. J., and C. L. Parkinson (2012), Arctic sea ice variability and trends, 1979–2010, *Cryosphere*, *6*(4), 881–889, doi:10.5194/tc-6–881-2012.

Condron, A., P. Winsor, C. Hill, and D. Menemenlis (2009), Simulated response of the Arctic freshwater budget to extreme NAO wind forcing, *J. Clim.*, *22*(9), 2422–2437, doi:10.1175/2008JCLI2626.1.

Fairall, C. W., E. F. Bradley, J. E. Hare, A. A. Grachev, and J. B. Edson (2003), Bulk parameterization of air-sea fluxes: Updates and verification for the COARE algorithm, *J. Clim.*, *16*(4), 571–591.

Gille, S. T. (2005), Statistical characterization of zonal and meridional ocean wind stress, *J. Atmos. Oceanic Technol.*, *22*(9), 1353–1372.

Guest, P. S., and K. L. Davidson (1991), The aerodynamic roughness of different types of sea ice, *J. Geophys. Res.*, *96*(C3), 4709–4721.

Hakkinen, S., A. Proshutinsky, and I. Ashik (2008), Sea ice drift in the Arctic since the 1950s, *Geophys. Res. Lett.*, *35*, L19704, doi:10.1029/2008GL034791.

Hibler, W. D. (1979), A dynamic thermodynamic sea ice model, *J. Phys. Oceanogr.*, *9*, 815–846.

Hibler, W. D., III, and K. Bryan (1987), A diagnostic ice-ocean model, *J. Phys. Oceanogr.*, *17*(7), 987–1015.

Hibler, W. D., A. Roberts, P. Heil, A. Y. Proshutinsky, H. L. Simmons, and J. Lovick (2006), Modeling M2 tidal variability in Arctic sea-ice drift and deformation, *Ann. Glaciol.*, *44*(1), 418–428.

Johnson, M., et al. (2012), Evaluation of Arctic sea ice thickness simulated by Arctic Ocean Model Intercomparison Project models, *J. Geophys. Res.*, *117*, C00D13, doi:10.1029/2011JC007257.

Kalnay, E., M. Kanamitsu, R. Kistler, W. Collins, D. Deaven, L. Gandin, M. Iredell, S. Saha, G. White, and J. Woollen (1996), The NCEP/NCAR 40-year reanalysis project, *Bull. Am. Meteorol. Soc.*, *77*(3), 437–471.

Kauker, F., R. Gerdes, M. Karcher, C. Köberle, and J. L. Lieser (2003), Variability of Arctic and North Atlantic sea ice: A combined analysis of model results and observations from 1978 to 2001, *J. Geophys. Res.*, *108*(C6), 3182, doi:10.1029/2002JC001573.

Kwok, R., and D. A. Rothrock (2009), Decline in Arctic sea ice thickness from submarine and ICESat records: 1958–2008, *Geophys. Res. Lett.*, *36*, L15501, doi:10.1029/2009GL039035.

Kwok, R., and N. Untersteiner (2011), The thinning of Arctic sea ice, *Phys. Today*, *64*(4), 36–41.

Kwok, R., E. C. Hunke, W. Maslowski, D. Menemenlis, and J. Zhang (2008), Variability of sea ice simulations assessed with RGPS kinematics, *J. Geophys. Res.*, *113*, C11012, doi:10.1029/2008JC004783.

Kwok, R., G. Spreen, and S. Pang (2013), Arctic sea ice circulation and drift speed: Decadal trends and ocean currents, *J. Geophys. Res. Oceans*, *118*, 2408–2425, doi:10.1002/jgrc.20191.

Large, W. G., and S. Pond (1981), Open ocean momentum flux measurements in moderate to strong winds, *J. Phys. Oceanogr.*, *11*(3), 324–336.

Levine, M. D., C. A. Paulson, and J. H. Morison (1987), Observations of internal gravity waves under the Arctic pack ice, *J. Geophys. Res.*, *92*(C1), 779–782.

Lindsay, R. W., and J. Zhang (2006), Assimilation of ice concentration in an ice-ocean model, *J. Atmos. Oceanic Technol.*, *23*(5), 742–749.

Losch, M., D. Menemenlis, J.-M. Campin, P. Heimbach, and C. Hill (2010), On the formulation of sea-ice models. Part 1: Effects of different solver implementations and parameterizations, *Ocean Modell.*, *33*(1), 129–144, doi:10.1016/j.ocemod.2009.12.008.

Lüpkes, C., V. M. Gryanik, J. Hartmann, and E. L. Andreas (2012), A parameterization, based on sea ice morphology, of the neutral atmospheric drag coefficients for weather prediction and climate models, *J. Geophys. Res.*, *117*, D13112, doi:10.1029/2012JD017630.

Martin, T., and R. Gerdes (2007), Sea ice drift variability in Arctic Ocean Model Intercomparison Project models and observations, *J. Geophys. Res.*, *112*, C04S10, doi:10.1029/2006JC003617.

McPhee, M. G. (1980), An analysis of pack ice drift in summer, in *Sea Ice Processes and Models*, edited by R. Pritchard, pp. 62–75, Univ. of Wash. Press, Seattle, Wash.

McPhee, M. G. (2002), Turbulent stress at the ice/ocean interface and bottom surface hydraulic roughness during the SHEBA drift, *J. Geophys. Res.*, *107*(C10), 8037, doi:10.1029/2000JC000633.

McPhee, M. G. (2012), Advances in understanding ice–ocean stress during and since AIDJEX, *Cold Reg. Sci. Technol.*, *76*, 24–36, doi:10.1016/j.coldregions.2011.05.001.

McPhee, M. G. (2013), Intensification of geostrophic currents in the Canada Basin, Arctic Ocean, *J. Clim.*, *26*(10), 3130–3138, doi:10.1175/JCLI-D-12-00289.1.

Morison, J. H., and M. McPhee (2001), Ice-ocean interaction, in *Encyclopedia of Ocean Sciences*, edited by J. Steele et al., pp. 1271–1281, Academic, London, doi:10.1006/rwos.2001.0003.
Morison, J. H., C. E. Long, and M. D. Levine (1985), Internal wave dissipation under sea ice, *J. Geophys. Res.*, *90*(C6), 11,959–11,966, doi:10.1029/JC090iC06p11959.
Nicolaus, M., C. Katlein, J. Maslanik, and S. Hendricks (2012), Changes in Arctic sea ice result in increasing light transmittance and absorption, *Geophys. Res. Lett.*, *39*, L24501, doi:10.1029/2012GL053738.
Nolin, A., R. L. Armstrong, and J. Maslanik (1998), *Near-Real-Time SSM/I-SSMIS EASE-Grid Daily Global Ice Concentration and Snow Extent*, Digital Media, Natl. Snow and Ice Data Cent., Boulder, Colo.
Overland, J. E. (1985), Atmospheric boundary layer structure and drag coefficients over sea ice, *J. Geophys. Res.*, *90*(C5), 9029–9049.
Parkinson, C. L., and W. M. Washington (1979), A large-scale numerical model of sea ice, *J. Geophys. Res.*, *84*(C1), 311–337, doi:10.1029/JC084iC01p00311.
Peralta-Ferriz, C., J. H. Morison, J. M. Wallace, and J. Zhang (2011), A basin-coherent mode of sub-monthly variability in Arctic Ocean bottom pressure, *Geophys. Res. Lett.*, *38*, L14606, doi:10.1029/2011GL048142.
Plueddemann, A. J., R. Krishfield, T. Takizawa, K. Hatakeyama, and S. Honjo (1998), Upper ocean velocities in the Beaufort Gyre, *Geophys. Res. Lett.*, *25*(2), 183–186.
Rainville, L., and R. A. Woodgate (2009), Observations of internal wave generation in the seasonally ice-free Arctic, *Geophys. Res. Lett.*, *36*, L23604, doi:10.1029/2009GL041291.
Rainville, L., C. Lee, and R. Woodgate (2011), Impact of wind-driven mixing in the Arctic Ocean, *Oceanography*, *24*(3), 136–145, doi:10.5670/oceanog.2011.65.
Rampal, P., J. Weiss, and D. Marsan (2009), Positive trend in the mean speed and deformation rate of Arctic sea ice, 1979–2007, *J. Geophys. Res.*, *114*, C05013, doi:10.1029/2008JC005066.
Rigor, I. G., and J. M. Wallace (2004), Variations in the age of Arctic sea-ice and summer sea-ice extent, *Geophys. Res. Lett.*, *31*, L09401, doi:10.1029/2004GL019492.
Schweiger, A., R. Lindsay, J. Zhang, M. Steele, H. Stern, and R. Kwok (2011), Uncertainty in modeled Arctic sea ice volume, *J. Geophys. Res.*, *116*, C00D06, doi:10.1029/2011JC007084.
Simmonds, I., and K. Keay (2009), Extraordinary September Arctic sea ice reductions and their relationships with storm behavior over 1979–2008, *Geophys. Res. Lett.*, *36*, L19715, doi:10.1029/2009GL039810.
Simmonds, I., and I. Rudeva (2012), The great Arctic cyclone of August 2012, *Geophys. Res. Lett.*, *39*, L23709, doi:10.1029/2012GL054259.
Spreen, G., R. Kwok, and D. Menemenlis (2011), Trends in Arctic sea ice drift and role of wind forcing: 1992–2009, *Geophys. Res. Lett.*, *38*, L19501, doi:10.1029/2011GL048970.
Steele, M., J. Zhang, D. Rothrock, and H. Stern (1997), The force balance of sea ice in a numerical model of the Arctic Ocean, *J. Geophys. Res.*, *102*(C9), 21,061–21,079.
Steele, M., W. Ermold, and J. Zhang (2008), Arctic Ocean surface warming trends over the past 100 years, *Geophys. Res. Lett.*, *35*, L02614, doi:10.1029/2007GL031651.
Taylor, P. K., and M. J. Yelland (2001), The dependence of sea surface roughness on the height and steepness of the waves, *J. Phys. Oceanogr.*, *31*(2), 572–590.
Thorndike, A. S., and R. Colony (1982), Sea ice motion in response to geostrophic winds, *J. Geophys. Res.*, *87*(C8), 5845–5852.
Yang, J. (2009), Seasonal and interannual variability of downwelling in the Beaufort Sea, *J. Geophys. Res.*, *114*, C00A14, doi:10.1029/2008JC005084.
Zhang, J., and D. A. Rothrock (2003), Modeling global sea ice with a thickness and enthalpy distribution model in generalized curvilinear coordinates, *Mon. Weather Rev.*, *131*(5), 845–861.
Zhang, J., and D. A. Rothrock (2005), Effect of sea ice rheology in numerical investigations of climate, *J. Geophys. Res.*, *110*, C08014, doi:10.1029/2004JC002599.
Zhang, J., M. Steele, R. Lindsay, A. Schweiger, and J. Morison (2008), Ensemble 1-year predictions of Arctic sea ice for the spring and summer of 2008, *Geophys. Res. Lett.*, *35*, L08502, doi:10.1029/2008GL033244.
Zhang, J., R. Lindsay, A. Schweiger, and I. Rigor (2012), Recent changes in the dynamic properties of declining Arctic sea ice: A model study, *Geophys. Res. Lett.*, *39*, L20503, doi:10.1029/2012GL053545.